Double-segregation effect in Ag_xPd_{1-x}/Ru(0001) thin film nanostructures

Tobias Marten,[1,*] Olle Hellman,[1] Andrei V. Ruban,[2] Weine Olovsson,[3] Charlotte Kramer,[4] Jan P. Godowski,[5] Lone Bech,[4] Zheshen Li,[6] Jens Onsgaard,[4] and Igor A. Abrikosov[1]

[1]*Department of Physics, Chemistry and Biology (IFM), Linköping University, SE-581 83 Linköping, Sweden*

[2]*Applied Materials Physics, Department of Materials Science and Engineering, Royal Institute of Technology, SE-100 44 Stockholm, Sweden*

[3]*Department of Materials Science and Engineering, Kyoto University, Kyoto 606-8501, Japan*

[4]*Department of Physics and Nanotechnology, Aalborg University, DK-9220 Aalborg East, Denmark*

[5]*Institute of Experimental Physics, University of Wroclaw, 50-204 Wroclaw, Poland*

[6]*Institute of Storage Ring Facilities, University of Aarhus, DK-8000 Aarhus, Denmark*

(Received 17 October 2007; published 7 March 2008)

We study the structural properties of ultrathin Ag_xPd_{1-x} films on top of a Ru(0001) substrate. Effective interatomic interactions, obtained from first-principles calculations, have been used in Monte Carlo simulations to derive the distribution of the alloy components in a four-monolayer (4-ML) Ag-Pd film. Though Ag-Pd alloys show complete solubility in the bulk, the thin film geometry leads to a pronounced segregation between Ag and Pd atoms with a strong preference of Ag atoms toward the surface and Pd atoms toward the interface. The theoretical prediction of this double-segregation effect is strongly supported by photoelectron spectroscopy experiments carried out for 4-ML thin films. We also show, in an additional experiment, that even in the case where initially 1 ML Ag is buried under 6 ML Pd, the whole Ag ML segregates to the surface.

DOI: 10.1103/PhysRevB.77.125406 PACS number(s): 79.60.Jv, 05.70.Np, 68.35.Dv, 71.15.−m

I. INTRODUCTION

Thin films grown on top of a substrate often possess new intriguing physical features. The electronic structure of thin films can differ quite radically from the bulk one due to the reduced dimensionality, surface relaxations, induced strain, etc. This leads to novel properties of the materials, which can be beneficial, e.g., in catalysis, for electronics and sensors. It is worth noticing that similar to bulk alloys one often specifies a nominal composition of the thin film alloy, tacitly assuming a uniform composition of the film. At the same time, several studies carried out for thin films consisting of metals, immiscible in their bulk forms, reported spontaneous formation of ordered domain patterns in the surface plane.[1–3] Ng and Vanderbilt[4] explained, using continuum elasticity models, that periodic surface structures could be stabilized through periodic stress domains. Another model was recently presented in Ref. 5 to describe structures with nanometer periodicity.

In this paper we study the opposite limit of thin film alloys by considering well-miscible elements: namely, AgPd on top of Ru(0001). AgPd systems are of interest by diverse applications, often related to the ability of Pd to adsorb high amounts of H_2, which, for instance, can be used to separate H_2 from a mixture of gases.[6] Ag and Pd have very small size mismatch (~5%), and in the bulk they mix over the whole concentration interval. We use a theoretically consistent way of determining the internal structure for the four-monolayer (4-ML) film by employing Monte Carlo simulations with effective interatomic interactions calculated from first principles. In order to check theoretical predictions, we carry out photoemission experiments on thin AgPd alloy films. We show that even in the case of alloys with complete solubility in the bulk the distribution of the alloy components in the thin film nanostructures may in general be nonuniform due to the double segregation of the different components toward the surface and the interface, respectively.

II. THEORETICAL METHODOLOGY AND DETAILS OF CALCULATIONS

Our theoretical technique is an extension of the method used with great success for the determination of the concentration profiles at alloy surfaces[7,8] towards the thin film alloys. The configurational part of the total energy in the finite-temperature statistical mechanics simulations is given by the Ising-type Hamiltonian, which in the case of an inhomogeneous (layered) system may be written as

$$H = \sum_{i\lambda} V_{\lambda}^{(1)} \sigma_{i\lambda} + \frac{1}{2} \sum_{i\lambda;j\lambda'} V_{\lambda\lambda';p(ij)}^{(2)} \sigma_{i\lambda}\sigma_{j\lambda'} + \cdots . \qquad (1)$$

Here $\sigma_{i\lambda}$ are spin variables, describing the alloy configuration and taking on values 1 if site i in the λ layer is occupied by Ag and −1 by Pd. $V_{\lambda}^{(1)}$ are the on-site interactions (chemical potentials) in layer λ proportional to the segregation energies in the corresponding layer in a homogeneous random equiatomic alloy; $V_{\lambda\lambda';p(ij)}^{(2)}$ are the effective pair interactions of type p between λ and λ' layers and lattice positions i and j in the corresponding layers.

In this work we assume that $V_{\lambda}^{(1)}$ are concentration independent, since the concentration dependence of the surface segregation energy in AgPd is very weak.[9] In this case the on-site interactions can be determined from the total energy of the equiatomic homogeneous random alloy as $V_{\lambda}^{(1)} = \partial E^{tot}/\partial\sigma_{\lambda}$. The effective pair interactions have been obtained by an *ab initio* screened version of the generalized perturbation method[10–12] (SGPM), which is a qualitative improvement on the earlier implementations of this theory.[13–15]

All the electronic structure calculations were performed within the density-functional theory[16,17] (DFT) using the Green's function technique[18–20] based on the method according to Korringa, Kohn, and Rostocker[21,22] (KKR) within the atomic sphere approximation[23,24] (ASA). The disorder effects were treated by means of the coherent potential approximation[25–31] (CPA). The KKR-ASA-CPA technique used in this work is described in detail in Ref. 18. The self-consistent solutions to the Kohn-Sham equations were carried out within the local density approximation (LDA), parametrized according to Perdew, Burke, and Ernzerhof,[32] using a basis set of *s*, *p*, *d*, and *f* ($l_{max}=3$) muffin-tin orbitals.[23,24] The multipole moment correction to the ASA Madelung one-electron potential and total energy[20,33] (ASA +M) have been used throughout all calculations. The Ag_xPd_{1-x} thin films are modeled by a continuation of the Ru(0001) stacking. In the simulations we also keep the sites of the underlying crystal lattice fixed to their ideal positions and we use the experimental lattice parameter of bulk Ru (2.70 Å). Based on earlier works carried out for the AgPd system,[19,34–36] we do not expect that the overall trends should be influenced by neglect of lattice relaxation effects. For the Monte Carlo simulations the 4-ML AgPd film has been modeled by a slab with periodic boundary conditions parallel to the surface and we have excluded the possibility of intermixing between the film and the substrate. This can be justified from the Ru-Ag and Ru-Pd phase diagrams,[37] both systems showing phase separation behavior up to very high temperatures. Besides, the surface segregation energy of Ru on the surface of Ag and Pd is very large,[18,38] and therefore it is very unlikely to have segregation of Ru atoms toward the surface.

We observed a strong dependence of the pair interactions on the concentration profile. In Fig. 1 we show the nearest-neighbor effective pair interactions within the surface layer, as well as the interaction between the surface layer and the deeper layers for four different arbitrarily chosen concentration profiles of the thin film. This is a quantum mechanical effect reflecting the sensitivity of the electronic structure to the local alloy composition, which is extremely difficult to model using a concentration-independent form of the Ising Hamiltonian. Therefore, we recalculate interactions during statistical thermodynamic simulations. We employ two methods to obtain the surface concentration profile, which we refer to as the self-consistent approach and the stepwise approach. The self-consistent method starts from choosing a concentration profile—for example, equiatomic composition in each surface layer λ. The interactions are then extracted from first-principles calculations and thereafter used in the Monte Carlo simulation to obtain a new profile. A mix of the old and new profiles is used as a new starting configuration to extract new pair interactions, rerun Monte Carlo simulations, and continue the procedure until self-consistency is achieved. The complementary method, the stepwise approach, starts from the same concentration profile—i.e., where there is no segregation—and runs Monte Carlo simulations for a high temperature down to a lower temperature where segregation starts to be significant. By monitoring the relative change in concentration for each layer while decreasing the temperature we obtain the dependence of the concentration profile on temperature, $c_\lambda(T)$. When $\Delta c_\lambda = c_\lambda(T') - c_\lambda(T) \approx 5\%$, for any $\lambda = 1, \ldots, 4$ and $T' < T$, the pair interactions are recalculated. This approach is slightly more time consuming since it relies on the previous temperature, whereas the self-consistent approach allows one to study concentration profiles at several different temperatures simultaneously. Both methods are schematically shown in Fig. 2. Note that although bulk Ru is absent in the statistical mechanics simulation of the concentration profile, the on-site and pair interactions are extracted in the presence of the Ru substrate. In our simulations we allow 8000 Monte Carlo steps per atom and collect and average physical quantities such as the total energy and concentration profiles over the last 5000 steps. The difference in energy between exchang-

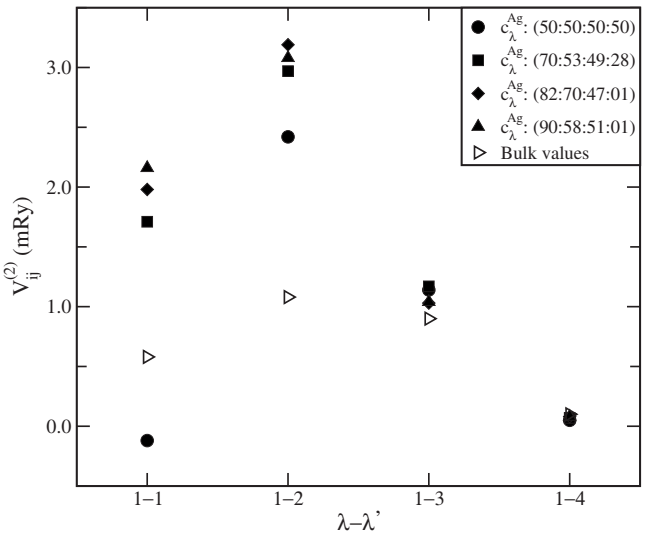

FIG. 1. Effective pair interactions between atoms in the surface layer λ=1 and nearest atoms in layer λ′ are calculated for four different, arbitrarily chosen, concentration profiles *c* of the 4-ML AgPd film (given in the inset, with compositions from the surface toward the Ru interface). In addition we present the bulk values for a $Ag_{50}Pd_{50}$ random alloy, which correspond to pairs of atoms, connected by the same vector as in the case of the film. For the sake of comparison we assume hcp structure for the bulk alloy.

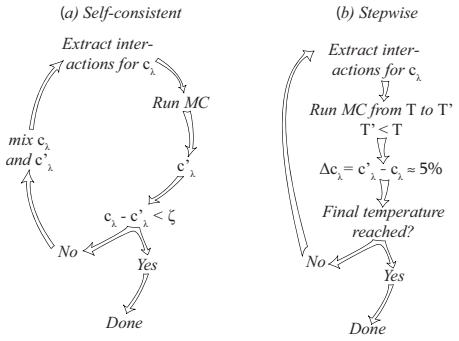

FIG. 2. Schematic illustration of the two computational approaches used to determine the concentration profiles for systems with concentration-dependent effective cluster interactions. The self-consistent and stepwise approaches are given in the left- and right-hand parts, respectively. See text for detailed discussion.

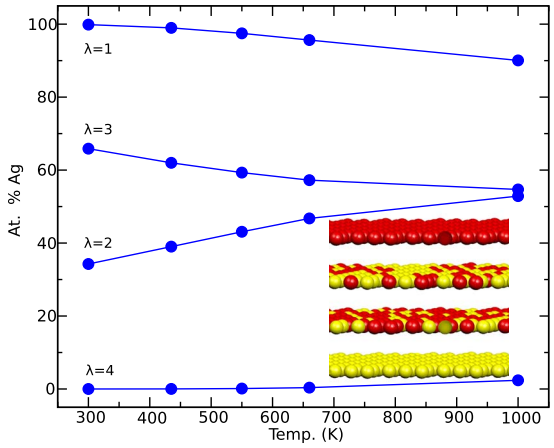

FIG. 3. (Color online) Surface concentration profiles for a 4-ML AgPd film supported by Ru(0001) as a function of temperature. $\lambda = 1, \ldots, 4$ denote the layers counted from the surface layer toward the interface layer. The distribution of the atoms at 660 K is shown in the inset (Ag, red; Pd, yellow).

ing two atoms was used, according to the asymmetric Metropolis algorithm.[39]

III. RESULTS AND DISCUSSION

A. Theoretical simulations

In Fig. 3 we show simulated concentration profiles obtained for a 4-ML AgPd film, with nominal equiatomic composition, deposited at a Ru(0001) substrate. Here we only show results obtained using the self-consistent approach, since the difference in the resulting concentration profile between the two approaches is less than 3 at. % Ag for all layers at all temperatures. We see an inhomogeneous distribution of alloy components across the film: a strong tendency of Ag segregation towards the surface and a similarly strong enrichment of Pd at the interface. Calculated effective cluster interactions of the Ising Hamiltonian, Eq. (1), clearly demonstrate that the structure of the 4-ML film is mainly determined by the chemical potential (on-site term). The enrichment at the surface can be explained by the difference in surface energies between Ag and Pd (the latter is higher than the former).[18,40] Indeed, $V_1^{(1)} = -7.40$ mRy (relative, say, to $V_2^{(1)} = 0.00$ mRy) is approximately equal to the surface energy difference of Ag and Pd. On the other hand, $V_4^{(1)} = 17.27$ mRy is proportional to the interface energy difference of Ag/Ru(0001) and Pd/Ru(0001). The lower value of the latter is due to much stronger interaction between Pd and Ru atoms than between Ag and Ru. Indeed, the Ag d band is almost completely occupied and therefore it cannot strongly participate in the bonding with d electrons of the substrate. On the contrary, unoccupied Pd d states can hybridize with Ru d electrons. This explains the enrichment of Pd at the interface.

At the same time the segregation energies in the two middle layers are small. Consequently, as seen from Fig. 3, the surface and the interface layers are almost saturated with Ag and Pd atoms, respectively, over the temperature range 300–1000 K (note that in the experiment Ag desorbs at temperatures above 870 K). Considering the two middle layers (denoted $\lambda = 2$ and 3) we see an almost equiatomic distribution of Ag and Pd at high temperatures. When the temperature decreases, Pd atoms start to segregate to the subsurface, while the Ag concentration in the third layer increases. This indicates a tendency to form alternating layers with Ag enrichment of the surface layer and a strong dominance of Pd at the interface.

Such a behavior reflects ordering trends present in the $Ag_{50}Pd_{50}$ system, which has a tendency to form the $L1_1$ structure as has been recently demonstrated in Refs. 9 and 41. Indeed, all variety of ordering behavior in alloys, isoelectronic to Ag-Pd, can be qualitatively understood from the results of the first two to three effective pair interactions. The main driving force for the $L1_1$ type of ordering in the bulk alloys is a weakening of the nearest-neighbor (NN) intralayer interaction (0.58 mRy in our case) and a relatively strong and positive NN interlayer interaction (1.08 and 1.19 mRy for NN and next-NN interactions, respectively). This sequence of interactions favors a tendency to form alternating Ag and Pd (0001) hcp or (111) fcc planes. To illustrate the difference on the ordering trends between the alloy surface and thin film alloy, we carried out self-consistent simulations of the segregation profile for the (111) surface of a fcc Ag-Pd alloy using the same setup and technique as for the Ag-Pd film deposited at the Ru(0001) surface. Note that exchange between atoms in the bulk and atoms at the surface (the four topmost layers) is permitted, and therefore the result shows a quantitative picture of the alloy surface concentration profile. Nevertheless, our simulations show that for the fcc (111) surface of $Ag_{50}Pd_{50}$ the surface-induced ordering takes place, with almost complete Ag occupation of the surface layer and Pd occupation of the subsurface layer up to 600 K, in agreement with earlier works.[42,43] Figure 4 shows the simulated

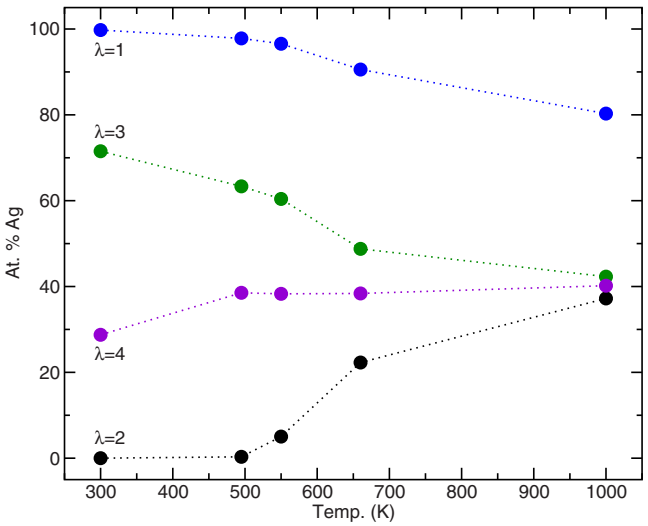

FIG. 4. (Color online) Self-consistent simulation of the segregation profile for the (111) surface of a fcc Ag-Pd alloy using the same setup and technique as for the Ag-Pd film. The notation is the same as in Fig. 3.

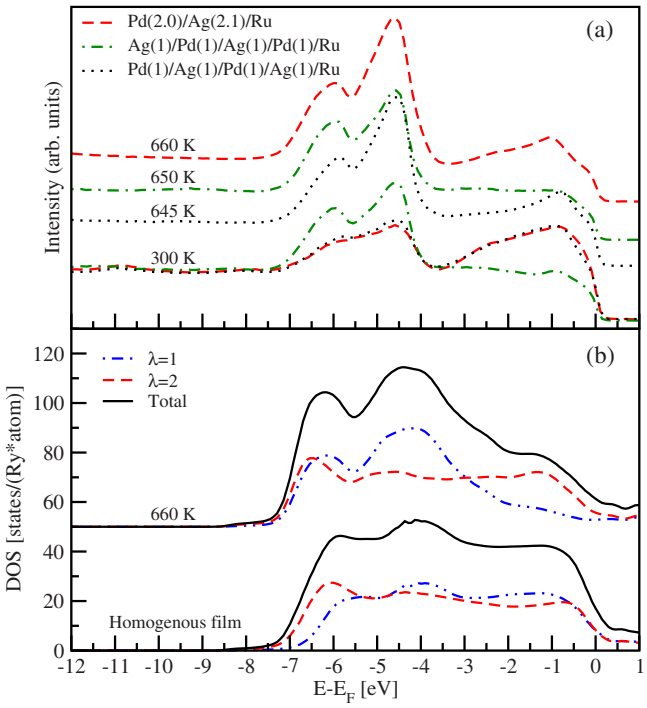

FIG. 5. (Color online) Comparison between (a) experimental valence band (VB) spectra and (b) theoretical VB density of states (DOS). (a) VB spectra of the Pd(2.0)/Ag(2.1)/Ru, Ag(1)/Pd(1)/Ag(1)/Pd(1)/Ru, and Pd(1)/Ag(1)/Pd(1)/Ag(1)/Ru interfaces at indicated temperatures. (b) Calculated layer-resolved VB-DOS for the surface and the subsurface layers as well as the total VB-DOS, which corresponds to the contribution from all layers accounting for the attenuation in the intensity through the layers—i.e., $\Sigma_{\lambda=1}^{4} w_{\lambda} \times \mathrm{DOS}(\lambda)$. The attenuation factor w_{λ} takes on values 1.00, 0.57, 0.33, and 0.19 for layers 1, 2, 3, and 4, respectively, and DOS(λ) denotes the calculated VB-DOS in layer λ.

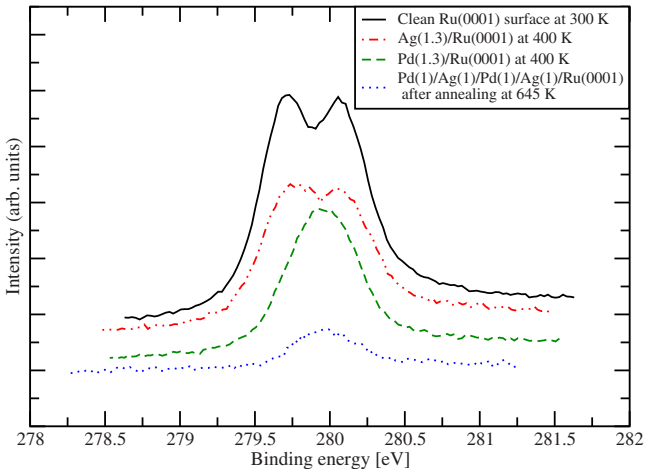

FIG. 6. (Color online) Ru $3d_{5/2}$ core level spectra recorded for an incoming photon energy of 350 eV. See text for discussion.

concentration profile of the alloy surface. One could expect that this ordering tendency increases in the thin film, because the observed double-segregation effect provides natural boundary conditions to form an ordered sequence of alternating Ag and Pd layers similar to a stacking of (111) planes in the $L1_1$ structure. However, Fig. 3 shows that this does not happen. Note that if one is not careful, one might think that the concentration profiles for the film and for the alloy surface are the same or very similar to each other. But as a matter of fact, the segregation profiles are qualitatively different between the surface of the alloy and the alloy film, as layers 2 and 4 are interchanged in Fig. 4, as compared to Fig. 3. This indicates that the surface-induced ordering of the $L1_1$ type, present at the alloy surface, is suppressed in the film. If we compare the same pair interactions as above for the film at 550 K (in mRy) ($V_{11;1}=2.66$, $V_{12;1}=3.20$, $V_{12;2}=1.45$; $V_{22;1}=1.00$, $V_{23;1}=1.10$, $V_{23;2}=0.91$; $V_{33;1}=0.28$, $V_{34;1}=-0.48$, $V_{34;2}=0.40$), we observe that the interactions are damped through the layers and that the NN interlayer interaction $V_{34;1}$ even changes sign. We conclude that the nanoscale thickness of the Ag-Pd alloy film is essential for the ordering behavior of the system, which differs drastically both from the bulk systems with complete solubility between Ag and Pd and from the surfaces of bulk alloys with a strong tendency toward $L1_1$-surface-induced order.

B. Comparison to experiment

In order to compare theory and experiment, thin Ag-Pd films were deposited on a Ru(0001) substrate and the core and valence band (VB) spectra were studied by photoelectron spectroscopy. Experimental data are based on the use of synchrotron radiation, from the storage ring ISA at Aarhus University, for measurements of the core-level shifts (CLSs) of the $3d_{5/2}$ electrons of Ru, Pd, and Ag. The photon energy was 40 eV for excitation of valence band electrons. The beamline is equipped with a spherical grating monochromator and a SCIENTA hemispherical concentric analyzer. Photons were incident at an angle of 40° with respect to the surface normal, and photoelectrons were collected by the 200-mm-mean-radius energy analyzer along the surface normal. The opening angle of the analyzer was ±9° and the total instrumental resolution was better than 0.2 eV and 0.1 eV for the $3d_{5/2}$ core electrons and valence band electrons, respectively. It was ensured that the kinetic energies of the emitted $3d$ electrons, around 60 eV, correspond to information from the first three to four atomic layers according to the exponential decay of the intensity with increasing depth. The facilities of the end station and the preparation of the Ru(0001) surface have been described earlier in Ref. 44. Calibrations of the Ag and Pd evaporation sources were based on photoelectron intensities, CLSs, and variations in the full widths at half maximum (FWHMs). The evaporation rate was in the order of 0.14 monolayers/min. Concerning the geometrical structure, low-energy electron diffraction (LEED) demonstrated the hexagonal patterns from the overlayers.

The 4-ML-thick Ag_xPd_{1-x} binary alloy film of the nominal composition $Ag_{50}Pd_{50}$ was formed by successive deposition of 1 ML of either Ag or Pd at 300 K on the Ru(0001) surface. In order to ensure that the films were as close as possible to the thermodynamic equilibrium extended annealing periods, of 30 min duration for temperatures below

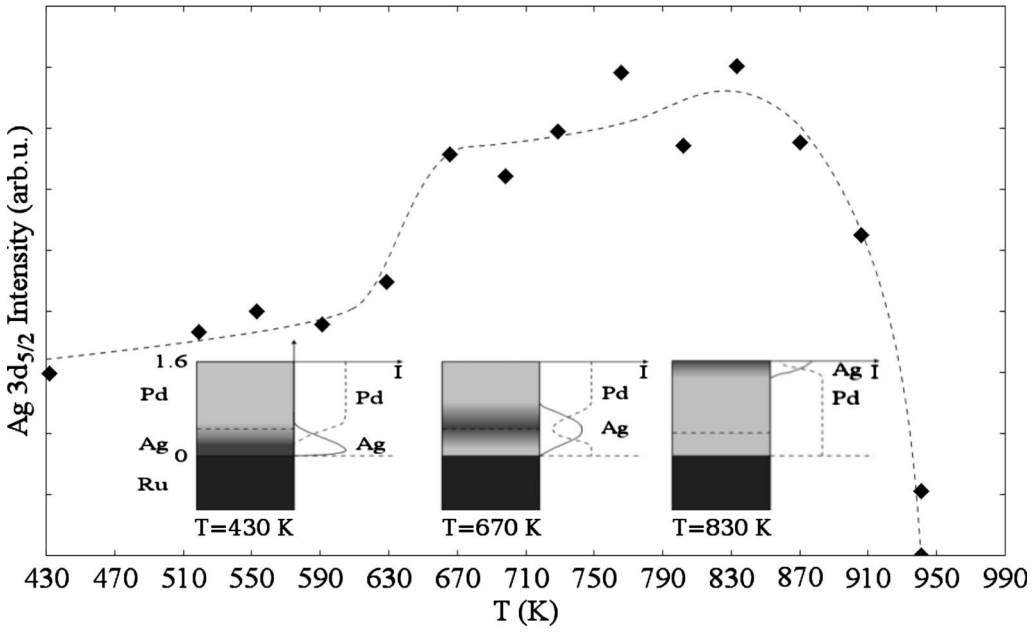

FIG. 7. Evolution of the Ag $3d_{5/2}$ intensity as a function of temperature for the Pd(6)/Ag(1)/Ru(0001) film. The insets show a schematic evolution of the concentration profile of Ag with temperature. At 430 K a smaller amount of Ag has diffused into the probing depth of the photoemission process. A substantial part of Ag has moved to the upper three layers at 670 K and primarily to the surface (concluded on the basis of the reduced Pd $3d_{5/2}$ signal, CLS of Ag, and VB-DOS). The maximum intensity, at 830 K, represents the segregation of Ag. The CLS of Ag shows a constant value in this temperature range, indicating a maximum Ag coordination number for the Ag atoms. Desorption of Ag takes place for $T>870$ K and no silver is observed for $T>940$ K.

500 K and 20 min for higher temperatures, were applied. It was also investigated whether the initial state of the film, which means the layer sequence, influences the final state. Consequently, three deposition sequences have been analyzed. Two of them, Ag(1)/Pd(1)/Ag(1)/Pd(1)/Ru(0001) and Pd(1)/Ag(1)/Pd(1)/Ag(1)/Ru(0001), are opposite in deposition sequence, and the third sandwich, studied in Ref. 45, Pd(2.0)/Ag(2.1)/Ru(0001), represents deposition of first 2.1 MLs of Ag followed by 2.0 MLs of Pd.

The nonpresence of Pd in the first layer is strongly supported by the VB energy distribution curves where the Ag 4*d* signal dominates the spectra at high temperatures; see Fig. 5. It is assessed that, inside the experimental uncertainty, the final states of the films are nearly the same. Further, the CLSs for the Ag $3d_{5/2}$ electrons are very close to each other comparing the different films. Valence band spectra of 4-ML-thick AgPd films with different deposition sequences, recorded at room temperature, are displayed in Fig. 5(a). It should be mentioned that the 4*d* cross sections for the two neighbor elements Pd and Ag are close lying.[46] It is observed that the two VB spectra of the Pd(1)/Ag(1)/Pd(1)/Ag(1)/Ru and Pd(2.0)/Ag(2.1)/Ru interfaces are almost identical with considerable intensity both in the low-binding energy range, with the Pd contribution, and in the Ag region around 5–8 eV binding energy, whereas the VB of the Ag(1)/Pd(1)/Ag(1)/Pd(1)/Ru film is dominated by the Ag 4*d* signal intensity even at 300 K. At temperatures around 650 K the VB energy distribution curves, Fig. 5(a), are strongly dominated by the Ag 4*d* signal and the Pd contribution in the first layer is distinctly reduced. Thus the theoretical prediction, the nonpresence of Pd in the first layer, is supported by the experiment. In Fig. 5 we also compare theoretical VB-DOS from the profile at 660 K to experimental VB spectra. Very good agreement is found for the binding energy (BE) positions of the DOS peaks of Ag, the span of the *d* band, and the contribution from Pd, which is observed close to the Fermi level, particularly for the film produced by the original deposition of Ag/Pd/Ag/Pd/Ru, which is the one closest to the theoretically predicted equilibrium structure. The Pd contribution originates from deeper layers as seen from the calculated layer-resolved DOS. Thus, this confirms our main theoretical predictions that Ag segregates toward the surface and Pd diffuses to the subsurface layers. On the other hand, strong evidence for the accumulation of Pd at the interface comes from the Ru $3d_{5/2}$ spectra as demonstrated in Fig. 6. The lower curve represents Ru $3d_{5/2}$ core electrons, transmitted through the overlayers, from the Pd(1)/Ag(1)/Pd(1)/Ag(1)/Ru(0001) sample after annealing at 645 K. It is clearly seen that the spectrum, with BE equal to 279.96 eV, line shape, and FWHM=0.49 eV, among the three possible interfaces included in the figure, fits with the Ru $3d_{5/2}$ core electrons from the Pd(1.3)/Ru(0001) interface. Further evidence comes from the Pd $3d_{5/2}$ spectrum that exhibits a distribution of several components. All CLSs in the following are referenced to 1 ML of the corresponding metal. Theoretical Pd $3d_{5/2}$ CLSs, calculated according to the complete screening picture,[34–36,47] gave −0.10 eV at $\lambda=2$ and $\lambda=3$—i.e., they are very close lying—and 0.29 eV at the interface with Ru. Experimentally, two peaks are observed at −0.33 eV and at 0.26 eV for the films around 650 K. Even though the CLSs differ somewhat for the Pd atoms in the middle layers, the Pd intensity, as deduced from experiment, is concentrated in lay-

ers 2, 3, and 4, in good agreement with theory.

In order to prove that the main driving force in forming nonuniform structures in thin Ag-Pd films on top of Ru is the strong layer dependence of the chemical potential of the alloy components, we carry out an additional experiment where initially, at room temperature, 1 ML Ag was buried under 6 MLs of Pd. Figure 7 shows the evolution of the intensity of the Ag $3d_{5/2}$ signal as a function of temperature. The determination of the intensity of the Ag $3d_{5/2}$ line is based on a fit with one peak. The BEs of surface and subsurface Ag $3d_{5/2}$ electrons (of clean Ag) are so close lying that they cannot be resolved. Since no change in the penetration depth of the electrons with temperature was observed for the 4-ML-thick Ag_xPd_{1-x} films, it is assumed that the probing depth is constant. Further, with a 70 eV kinetic energy of the emitted Ag $3d$ electrons, a maximal surface sensitivity is obtained. Accordingly, the intensity variation with temperature reflects the Ag occupation in the surface. Three distinct temperature regimes are observed. Diffusion of Ag takes place for temperatures between 590 K and 670 K. Then an approximately constant intensity level, the segregation state, is observed for temperatures up to 830 K. The third temperature regime, the desorption region, lasts to 940 K where all the Ag atoms have desorbed. Only in the diffusion region can a broader FWHM of the Ag $3d$ peak be observed, indicating the strongly varying coordination number of Ag through the layers. It is noted that some Ag signal is observed even at room temperature, although the layer-by-layer deposition of Pd should quench the Ag signal due to attenuation. In a kinematic description the buildup of Ag in the uppermost three layers can be described as "an impulse" of silver moving toward the surface with increasing temperature, illustrated in the inset in Fig. 7, where the three sandwiches show, in a schematic way, the evolution of the concentration profile of silver with temperature.

IV. SUMMARY

To summarize we have shown that, in contrast to the complete solubility between Ag and Pd which takes place in the bulk alloys, the alloy components are distributed nonuniformly across the growth direction in the thin film, with the strong double segregation of Ag and Pd toward the surface and the interface, respectively, and suppressed surface-induced $L1_1$ ordering, present at the surface of bulk alloys. We suggest that the double-segregation phenomenon is general for thin alloy films between elements which form solid solutions in the bulk, but have a large difference in surface energies.

ACKNOWLEDGMENTS

The Swedish Research Council (VR), the Swedish Foundation for Strategic Research (SSF), and NordForsk are acknowledged for financial support. Calculations have been performed at the National Supercomputer Centre (NSC) in Linköping, Sweden.

*tobma@ifm.liu.se

[1] E. D. Tober, R. C. F. Farrow, R. F. Marks, G. Witte, K. Kalki, and D. D. Chambliss, Phys. Rev. Lett. **81**, 1897 (1998).
[2] B. Sadigh, M. Asta, V. Ozoliņš, A. K. Schmid, N. C. Bartelt, A. A. Quong, and R. Q. Hwang, Phys. Rev. Lett. **83**, 1379 (1999).
[3] G. E. Thayer, V. Ozolins, A. K. Schmid, N. C. Bartelt, M. Asta, J. J. Hoyt, S. Chiang, and R. Q. Hwang, Phys. Rev. Lett. **86**, 660 (2001).
[4] K.-O. Ng and D. Vanderbilt, Phys. Rev. B **52**, 2177 (1995).
[5] V. Ozoliņš, M. Asta, and J. J. Hoyt, Phys. Rev. Lett. **88**, 096101 (2002).
[6] L. C. Witjens, J. H. Bitter, A. J. van Dillen, K. P. de Jong, and F. M. F. de Groot, Phys. Chem. Chem. Phys. **6**, 3903 (2004).
[7] L. V. Pourovskii, A. V. Ruban, I. A. Abrikosov, Y. Kh. Vekilov, and B. Johansson, Phys. Rev. B **64**, 035421 (2001).
[8] L. V. Pourovskii, A. V. Ruban, B. Johansson, and I. A. Abrikosov, Phys. Rev. Lett. **90**, 026105 (2003).
[9] A. V. Ruban, S. I. Simak, P. A. Korzhavyi, and B. Johansson, Phys. Rev. B **75**, 054113 (2007).
[10] A. V. Ruban and H. L. Skriver, Phys. Rev. B **66**, 024201 (2002).
[11] A. V. Ruban, S. I. Simak, P. A. Korzhavyi, and H. L. Skriver, Phys. Rev. B **66**, 024202 (2002).
[12] A. V. Ruban, S. Shallcross, S. I. Simak, and H. L. Skriver, Phys. Rev. B **70**, 125115 (2004).
[13] V. Drchal, J. Kudrnovský, L. Udvardi, P. Weinberger, and A. Pasturel, Phys. Rev. B **45**, 14328 (1992).
[14] A. Pasturel, V. Drchal, J. Kudrnovský, and P. Weinberger, Phys. Rev. B **48**, 2704 (1993).
[15] V. Drchal, A. Pasturel, R. Monnier, J. Kudrnovský, and P. Weinberger, Comput. Mater. Sci. **15**, 144 (1999).
[16] P. Hohenberg and W. Kohn, Phys. Rev. **136**, B864 (1964).
[17] W. Kohn and L. J. Sham, Phys. Rev. **140**, A1133 (1965).
[18] A. V. Ruban and H. L. Skriver, Comput. Mater. Sci. **15**, 119 (1999).
[19] I. A. Abrikosov and H. L. Skriver, Phys. Rev. B **47**, 16532 (1993).
[20] H. L. Skriver and N. M. Rosengaard, Phys. Rev. B **43**, 9538 (1991).
[21] J. Korringa, Physica (Amsterdam) **13**, 392 (1947).
[22] W. Kohn and N. Rostoker, Phys. Rev. **94**, 1111 (1954).
[23] O. K. Andersen, Phys. Rev. B **12**, 3060 (1975).
[24] O. K. Andersen and O. Jepsen, Phys. Rev. Lett. **53**, 2571 (1984).
[25] P. Soven, Phys. Rev. **156**, 809 (1967).
[26] B. Velický, S. Kirkpatrick, and H. Ehrenreich, Phys. Rev. **175**, 747 (1968).
[27] S. Kirkpatrick, B. Velický, and H. Ehrenreich, Phys. Rev. B **1**, 3250 (1970).
[28] B. L. Györffy, Phys. Rev. B **5**, 2382 (1972).
[29] J. S. Faulkner and G. M. Stocks, Phys. Rev. B **21**, 3222 (1980).
[30] J. S. Faulkner, Prog. Mater. Sci. **27**, 1 (1982).
[31] B. L. Gyorffy and G. M. Stocks, Phys. Rev. Lett. **50**, 374 (1983).
[32] J. P. Perdew, K. Burke, and M. Ernzerhof, Phys. Rev. Lett. **77**,

3865 (1996).
[33] P. A. Korzhavyi, I. A. Abrikosov, B. Johansson, A. V. Ruban, and H. L. Skriver, Phys. Rev. B **59**, 11693 (1999).
[34] I. A. Abrikosov, W. Olovsson, and B. Johansson, Phys. Rev. Lett. **87**, 176403 (2001).
[35] W. Olovsson, L. Bech, T. H. Andersen, Z. Li, S. V. Hoffmann, B. Johansson, I. A. Abrikosov, and J. Onsgaard, Phys. Rev. B **72**, 075444 (2005).
[36] T. Marten, W. Olovsson, S. I. Simak, and I. A. Abrikosov, Phys. Rev. B **72**, 054210 (2005).
[37] T. B. Massalski, *Binary Alloy Phase Diagram*, 2nd ed. (ASM International, Materials Park, OH, 1990), Vol. 2.
[38] A. V. Ruban, H. L. Skriver, and J. K. Nørskov, Phys. Rev. B **59**, 15990 (1999).
[39] K. Binder, *Applications of the Monte-Carlo Method in Statistical Physics* (Springer, Berlin, 1984).
[40] H. L. Skriver and N. M. Rosengaard, Phys. Rev. B **46**, 7157 (1992).
[41] S. Müller and A. Zunger, Phys. Rev. Lett. **87**, 165502 (2001).
[42] P. T. Wouda, M. Schmid, B. E. Nieuwenhuys, and P. Varga, Surf. Sci. **417**, 292 (1998).
[43] M. Ropo, Phys. Rev. B **74**, 195401 (2006).
[44] T. H. Andersen, L. Bech, Z. Li, S. V. Hoffmann, and J. Onsgaard, Surf. Sci. **559**, 111 (2004).
[45] L. Bech, Z. Li, and J. Onsgaard, J. Electron Spectrosc. Relat. Phenom. **156-158**, 102 (2007).
[46] J. J. Yeh and I. Lindau, At. Data Nucl. Data Tables **32**, 1 (1985).
[47] B. Johansson and N. Mårtensson, Phys. Rev. B **21**, 4427 (1980).